Simulation of electromagnetically and magnetically induced transparency in a magnetized plasma

M. S. Hur, J. S. Wurtele, and G. Shvets

Simulation of electromagnetically and magnetically induced transparency in a magnetized plasma

M. S. Hur
University of California, Berkeley, Berkeley, California 94720

J. S. Wurtele
University of California, Berkeley and Lawrence Berkeley National Laboratory, Berkeley, California 94720

G. Shvets
*Illinois Institute of Technology, Chicago, Illinois 60616
and Fermi National Accelerator Laboratory, Batavia, Illinois 60510*

Electromagnetically induced transparency (EIT), a phenomenon well known in atomic systems, has a natural analogy in a classical magnetized plasma. The magnetized plasma has a resonance for right-hand polarized electromagnetic waves at the electron cyclotron frequency Ω_0, so that a probe wave with frequency $\omega_1 = \Omega_0$ cannot propagate through the plasma. The plasma can be made transparent to such a probe by the presence of a pump wave. The pump may be an electromagnetic wave or magnetostatic wiggler. Simulations and theory show that the physical reason for the transparency is that the beating of the probe wave with the pump wave sets up a plasma oscillation, and the upper sideband of the pump wave cancels the resonant plasma current due to the probe. The theory of plasma EIT derived here extends that found in the earlier work to include the effects of the lower sideband of the pump and renormalization of the plasma frequency and an analysis of the transient response. A detailed comparison of theory to one-dimensional particle-in-cell simulations is presented and estimates for the performance ion accelerator using the EIT interaction are given. The dispersion relation and estimates for the phase velocity and amplitude of the plasma wave are in good agreement with particle-in-cell simulations. © *2003 American Institute of Physics.* [DOI: 10.1063/1.1580816]

I. INTRODUCTION

Electromagnetically induced transparency (EIT) is a well-known[1,2] quantum phenomenon which is interesting from an academic point of view and of use for various applications.[3,4] It was recently proposed[5,6] that a magnetized plasma can be used to realize a classical analogy of quantum EIT. In the classical EIT system considered here, a magnetized plasma can be made transparent to a right-hand polarized probe wave with a frequency resonant with the cyclotron frequency. This is accomplished by the presence of a strong, appropriately detuned, pump wave. The basic idea is to use the sideband of the pump to cancel the resonant response of electrons to the probe. This is conceptually similar to the quantum EIT in a three-state atomic system where the transparency is induced by the destructive interference between several pathways which connect the ground and the excited states. Transparency can be induced, as well, by a static helical magnetic wiggler.[6–8] The wiggler acts as a zero frequency pump wave.

The idea of realizing induced transparency in a plasma is not new. Previous work[9–11] examined induced transparency in unmagnetized plasmas. These papers considered a pump wave induced transparency for a probe beam that is cut-off ($\omega_{\text{probe}} < \omega_p$). The analysis was based on three-wave and four-wave interactions. The system did not share many of the basic features of quantum EIT. For example, transparency of the probe was induced near a cut-off, not a resonance, and transparency was induced using a pump with a higher frequency than that of the probe. Furthermore, the rather precise correspondence between the magnetized plasma EIT dispersion relation and quantum EIT is not found in studies of unmagnetized plasma transparency.

One of the potential applications of the magnetized plasma EIT system is as an advanced accelerator for ions. Plasma-based advanced accelerators, in which the accelerating structure is generated from the interaction between a plasma and a high intensity laser pulse or a relativistic electron beam, have been the subject of intensive study.[12] In the laser beat wave and wake field schemes, as well as the beam-driven wake field, the plasma wave has a phase velocity nearly the speed of light. Thus, it is useful for accelerating electrons, but not proper for non-relativistic heavy particle acceleration. In contrast, a plasma wave generated in the EIT system has numerous properties desirable for a heavy particle accelerator. The simulated accelerating gradient is of order 4×10^7 V/m for realizable 1 T solenoidal fields. The phase velocity is slow, which makes it possible to trap non-relativistic heavy particles. Furthermore, the phase velocity is readily controlled by adjusting the wiggler wavelength. Resonance with the cyclotron frequency implies, for typical parameters, electromagnetic waves in the microwave frequency region.

This paper is organized as follows. Section II reviews the basic theory of our concept, expanding on a shorter version of the theory presented elsewhere.[6] In Sec. III, we investigate detailed properties of EIT using a one-dimensional particle-in-cell (PIC) simulation and compare the simulations with theory. In Sec. IV, the application of EIT as an advanced accelerator is discussed. A summary is given in the last section.

II. BASIC CONCEPT AND FORMALISM

A. Analysis of the steady-state motion

We consider a magnetized plasma with density n_0 and external magnetic field $\mathbf{B}_0 = B_0 \mathbf{e}_z$. The dispersion relation of a right-hand polarized electromagnetic wave (probe) is

$$\omega_1^2 = c^2 k^2 + \omega_p^2 \frac{\omega_1}{\omega_1 - \Omega_0}, \tag{1}$$

where $\omega_p = \sqrt{4\pi n_0 e^2/m}$, $\Omega_0 = eB_0/mc$, m is the electron mass, e the electron charge, and c is the speed of light. The dispersion relation has a band gap between Ω_0 and $\Omega_0/2 + \sqrt{\Omega_0^2/4 + \omega_p^2}$, where the probe transmission is prohibited. Since a large transverse electron current is resonantly excited at $\omega_1 = \Omega_0$, most of the probe energy is absorbed in the plasma. Following the calculation outlined in Ref. 6, we show that when there exists a pump electromagnetic wave, the electron transverse current can be suppressed by a sideband of the pump field induced by longitudinal electron motion in the beat wave of the pump and probe. In the presence of the ponderomotive potential produced by the beat between the probe and the pump, electrons move longitudinally, with their positions and velocities varying as $e^{-i\Delta\omega t + i\Delta k z}$, where $\Delta\omega$ (Δk) is the beat frequency (wavenumber) between the pump and the probe. The pump electric field, as seen by a given slice of plasma, is approximated as $\mathbf{E}_{\text{pump}}(z,t) \sim \mathbf{E}_{\text{pump}}(z_0,t) + \zeta \times \partial_z \mathbf{E}_{\text{pump}}$, where $z = z_0 + \zeta$, z_0 represents the initial position of the slice, and ζ is its longitudinal displacement. The second term couples the longitudinal motion and the transverse field, thereby inducing sidebands at frequencies $\omega_0 \pm \Delta\omega$. The Lorentz force $(-e/c)\dot{\zeta} \times \mathbf{B}_{\text{pump}}$ also couples the pump and the longitudinal motion producing the sidebands at the same frequencies. A critical aspect of induced transparency in plasma is that the perpendicular electron motion due to the probe electric field is canceled by the response to the upper sideband (which is at the probe frequency).

The above-described process can be shown mathematically by a steady-state analysis of electron motion in an axial magnetic field $B_0 \mathbf{e}_z$ and perpendicular electromagnetic fields of the pump and the probe.[6,7] The non-relativistic equations of motion are

$$\frac{d\mathbf{v}_\perp}{dt} = -\frac{e}{m}\left(\mathbf{E}_\perp + \frac{\mathbf{v}_\perp \times B_0 \mathbf{e}_z}{c} + \frac{\dot{\zeta}\mathbf{e}_z \times \mathbf{B}_\perp}{c} \right) \tag{2}$$

and

$$\ddot{\zeta} + \omega_p^2 \zeta = -\frac{e}{mc}\mathbf{v}_\perp \times \mathbf{B}_\perp, \tag{3}$$

where $\mathbf{E}_\perp$ and $\mathbf{B}_\perp$ are the combined fields of the pump and the probe, and ζ is the longitudinal plasma displacement from the initial position z_0. The $\omega_p^2 \zeta$ term on the left-hand side of Eq. (3) is due to the restoring force of the neutralizing immobile ion background. The perpendicular fields are given by

$$2e\mathbf{E}_{\perp 0,1}/mc\omega_{0,1} = a_{0,1}\mathbf{e}_+ \exp(i\bar{\theta}_{0,1}) + \text{c.c.} \tag{4}$$

and

$$\mathbf{B}_{\perp 0,1} = (c\mathbf{k}_{0,1}/\omega_{0,1}) \times \mathbf{E}_{\perp 0,1}, \tag{5}$$

where $a_{0,1}$ are normalized vector potentials ($a_{0,1} = eA_{0,1}/mc^2$), $\mathbf{e}_\pm = \mathbf{e}_x \pm i\mathbf{e}_y$, $\bar{\theta}_{0,1} = k_{0,1}z - \omega_{0,1}t$, and the subscripts 0 and 1 refer to the pump and the probe, respectively. For convenience, we use $\mathbf{e}_\pm$ as unit vectors of a new coordinate system. The perpendicular velocity is expanded as $\boldsymbol{\beta}_\perp = \mathbf{v}_\perp/c = (\beta_+ \mathbf{e}_+ + \beta_- \mathbf{e}_-)/2$, where $\beta_\pm = (v_x \mp iv_y)/c$.

Assuming a weak probe ($a_1 \ll a_0$) and perturbative longitudinal motion ($k_{0,1}\zeta \ll 1$), we linearize Eqs. (2) and (3) in ζ and a_1 as

$$\dot{\beta}_+ + i\Omega_0 \beta_+ = -\omega_0 a_0 e^{i\theta_0}(1 + ik_0\zeta - k_0\dot{\zeta}/\omega_0) \\ - \omega_1 a_1 e^{i\theta_1}, \quad \beta_- = \beta_+^*, \tag{6}$$

$$\ddot{\zeta} + \omega_p^2 \zeta = -\frac{c^2}{2}(k_0 a_0 \beta_- e^{i\theta_0} + k_1 a_1 \beta_- e^{i\theta_1} \\ + ik_0^2 \zeta \beta_- a_0 e^{i\theta_0}) + \text{c.c.}, \tag{7}$$

where $\Omega_0 = eB_0/mc$. The eikonal term was approximated as $e^{i\bar{\theta}_{0,1}} \simeq e^{i\theta_{0,1}}(1 + ik_{0,1}\zeta)$, where $\theta_{0,1} = k_{0,1}z_0 - \omega_{0,1}t$. The longitudinal motion in the ponderomotive beat potential is

$$\zeta = \frac{\tilde{\zeta}}{2}e^{i(\theta_1 - \theta_0)} + \frac{\tilde{\zeta}^*}{2}e^{-i(\theta_1 - \theta_0)}. \tag{8}$$

The largest amplitude of ζ is generated when the pump frequency, ω_0, is detuned from the probe frequency by $\Delta\omega = \omega_1 - \omega_0 \approx \omega_p$. The beatwave resonance condition $\Delta\omega \approx \omega_p$ is satisfied only approximately because of the renormalization of the plasma frequency from its ω_p value, as explained in the following.

Substituting Eq. (8) into Eq. (6) yields a steady-state solution for β_+:

$$\beta_+ = -\frac{i\omega_0 a_0}{\omega_0 - \Omega_0}e^{i\theta_0} - \frac{i\omega_1}{\omega_1 - \Omega_0}\left(a_1 + \frac{ik_0\tilde{\zeta}}{2}a_0 \right)e^{i\theta_1} \\ - \frac{(\omega_1 - 2\omega_0)a_0}{2\omega_0 - \omega_1 - \Omega_0}\frac{k_0\tilde{\zeta}^*}{2}e^{-i\theta_1 + 2i\theta_0}. \tag{9}$$

The first term on the right-hand side (RHS) of Eq. (9) is the electron response to the electric field of the pump. This term vanishes if the pump is a magnetostatic wiggler ($\omega_0 = 0$). The second term on the RHS of Eq. (9) is the electron response to the electromagnetic fields of the probe ($\sim a_1 e^{i\theta_1}$) and the upper sideband ($\sim ia_0\zeta e^{i\theta_1}$) of the pump. The last term on the RHS of Eq. (9) is due to the lower sideband of the pump at $\omega_0 - \Delta\omega$. In the case of a magnetostatic wiggler, this term represents the left-hand polarized component

of the electron velocity. It arises because the magnetic force of the wiggler acting on a longitudinal plasma wave (proportional to ζ) has two components: a resonant right-hand polarized and a non-resonant left-hand polarized one. It is important to note that a finite solution exists at resonance ($\omega_1 = \Omega_0$) when

$$a_1 + \frac{ik_0\tilde{\zeta}}{2}a_0 = 0. \tag{10}$$

Equation (10) represents the suppression of the probe by the pump. It can be shown that Eq. (10) gives a stable steady-state solution for $\tilde{\zeta}$ which is adiabatically reached by slowly turning on the probe in the presence of the pump. The steady-state solution is reached only if the plasma is initially quiescent. Single particle simulations[6] lead to the same conclusion.

Next we consider the general case of $\omega_1 \neq \Omega_0$. We fix the pump detuning at $\omega_p = \Omega_0 - \omega_0$. Substituting Eq. (9) into Eq. (7), and writing the time derivative as $\partial_t = -i\Delta\omega$, yields

$$\beta_+ = -\frac{i\omega_0 a_0}{\omega_0 - \Omega_0}e^{i\theta_0} - \frac{i\omega_1 a_1}{\omega_0 - \Omega_0}e^{i\theta_1}\frac{c^2 k_0^2 |a_0|^2 \omega_0(k_1/k_0 - 2 - X) + 2(\omega_p^2 - \Delta\omega^2)(\omega_0 - \Omega_0)}{c^2 k_0^2 |a_0|^2 \omega_1 + 2(\omega_p^2 - \Delta\omega^2)\delta\Omega}$$

$$+ \frac{i(\omega_1 - 2\omega_0)a_1^*}{2\omega_0 - \omega_1 - \Omega_0}e^{-i\theta_1 + 2i\theta_0}\frac{c^2 k_0^2 a_0^2 \omega_1}{c^2 k_0^2 a_0^2 \omega_1 + 2(\omega_p^2 - \Delta\omega^2)\delta\Omega}, \tag{12}$$

where

$$\delta\Omega = \omega_1 - \Omega_0 \tag{13}$$

and

$$X = \frac{(\omega_1 - 2\omega_0)(\omega_0 - \Omega_0)}{\omega_0(2\omega_0 - \omega_1 - \Omega_0)}. \tag{14}$$

We ignored $O(\delta\Omega^3)$ in the denominators of each term in Eq. (12). For simplicity, we also neglected terms proportional to the product of $|a_0|^2$ and $\delta\Omega$. This is possible since $|a_0|$ is of same order as $\delta\Omega/\Omega_0$ near the new resonance between the probe and the EIT plasma, which is verified as follows: The denominator of the second term in Eq. (12) can be simplified for $\delta\Omega/\Omega_0 \ll 1$ as $D = c^2 k_0^2 |a_0|^2 \omega_1 + 2(\omega_p^2 - \Delta\omega^2)\delta\Omega \simeq 4\omega_p(\Omega_R^2 - \delta\Omega^2)$, where $\Omega_R = ck_0|a_0| \times \sqrt{\Omega_0/4\omega_p}$ is the effective Rabi frequency. The plasma is resonantly driven for $D = 0$, which occurs when $\omega_1 = \Omega_0 \pm \Omega_R$. Hence, the resonance of the magnetized plasma is shifted by the pump, and a new transparency band is generated between $\Omega_0 - \Omega_R$ and $\Omega_0 + \Omega_R$. For typical parameters of $\Omega_0/\omega_p \sim 4$ and $ck_0 \sim \omega_0$, the Rabi frequency is approximately $\omega_0|a_0|$. Hence the normalized detuning $\delta\Omega/\Omega_0$ near the resonance becomes $|a_0|\omega_0/\Omega_0$, where $\omega_0/\Omega_0 \sim 1$. When the probe, pump, and plasma frequencies match each other exactly ($\delta\Omega \sim 0$), all the terms including $\delta\Omega$ may be ignored. Therefore, neglecting $|a_0|^2 \delta\Omega$ is a good approximation

$$(\omega_p^2 - \Delta\omega^2)\tilde{\zeta} = ic^2\left[\frac{k_0 a_0^* \omega_1}{\omega_1 - \Omega_0}\left(a_1 + \frac{ik_0\tilde{\zeta}a_0}{2}\right) - \frac{k_1 a_1 \omega_0}{\omega_0 - \Omega_0}a_0^*\right.$$

$$\left. -i\frac{k_0^2 \tilde{\zeta}\omega_0}{\omega_0 - \Omega_0}|a_0|^2 - \frac{i}{2}\frac{k_0^2 \tilde{\zeta}(\omega_1 - 2\omega_0)}{(2\omega_0 - \omega_1 - \Omega_0)}|a_0|^2\right]. \tag{11}$$

Note that the second and third terms in the square brackets vanish for the magnetostatic pump. The fourth term in the square brackets (which does not vanish even for $\omega_0 = 0$) describes the renormalization of the plasma frequency due to the presence of the pump. As previously mentioned, the interaction of the pump with the plasma wave gives rise to the non-resonant left-handed electron rotation. This rotation, in turn, couples with the pump so as to produce a longitudinal force on the electron. For a magnetostatic pump there results a renormalized plasma frequency given by $\bar{\omega}_p^2 = \omega_p^2 + k_0^2 c^2 |a_0|^2/4$.

Eliminating $\tilde{\zeta}$ from Eqs. (9) and (11) gives the steady-state perpendicular motion. We retain the $e^{i\theta_1}$ and $e^{i\theta_0}$ components of β_+, resulting in

in the two most interesting regimes. Note that the term X did not appear in the original theory.[6] We expect there to be only a minor change from Ref. 6 near the EIT resonance at $\omega_1 \simeq \Omega_0$. The lower sideband contains the physics of the Raman instability of the pump for the case $\omega_1 \sim \omega_0 - \omega_p$. Furthermore, we have checked that including this term results in only a small shift of the dispersion curve toward larger k_1. For example, for a magnetostatic pump, complete transparency ($\omega_1 = k_1 c$) is achieved when $\omega_1 = \Omega_0 = \bar{\omega}_p$.

The dispersion relation of the probe is derived from the wave equation:

$$(\partial_t^2 - c^2\partial_z^2)E_+ = -4\pi\partial_t J_+ = 4\pi e n_0 \partial_t u_+, \tag{15}$$

where E_+ is the probe electric field, J_+ the right-hand polarized $e^{i\theta_1}$ component of the current, n_0 the unperturbed plasma density, and u_+ the fluid velocity of the plasma. The fluid velocity u_+ is derived from the single electron velocity β_+. Any electron with its initial position z_0 and its longitudinal displacement ζ contributes to the fluid velocity at $z = z_0 + \zeta$. Hence, the fluid velocity is given by $u_+/c = b_+(z) = \int_{-\infty}^{\infty}dz_0\beta_+(z_0)\delta(z - z_0 - \zeta) \simeq \beta_+ - \partial_z(\zeta\beta_+)$. Using this formula and Eqs. (8) and (12), we calculate the $e^{i\theta_1}$ component of the fluid velocity:

$$b_+ = i\omega_1 a_1 e^{i\theta_1}\frac{\delta\Omega + \delta\Omega_0(k_1)}{\Omega_R^2 - \delta\Omega^2}, \tag{16}$$

where $\delta\Omega_0(k_1) = (2\omega_0\Omega_R^2/\omega_p\Omega_0)(k_1/k_0 - 1 - X/2)$. Substituting Eq. (16) into Eq. (15) yields

$$\omega_1^2 = c^2k_1^2 - \omega_p^2\omega_1\frac{\delta\Omega + \delta\Omega_0(k_1)}{\Omega_R^2 - \delta\Omega^2}. \tag{17}$$

As expected, Eq. (17) reduces to the R-polarized dispersion relation of a single wave in a magnetized plasma for $\delta\Omega \gg \Omega_R$.

The pump wave can be replaced by a helical magnetic wiggler with wavelength λ_w. In this case, the wiggler corresponds to a pump with zero-frequency and wavenumber $k_w = 2\pi/\lambda_w$. Therefore, the frequency matching condition should be $\omega_p = \omega_1 - \omega_0 = \omega_1$. The wiggler is modeled in a one-dimensional limit as

$$\mathbf{B}_w \simeq \frac{mc\Omega_w}{2e}e^{\mp ik_wz}\mathbf{e}_+ + \text{c.c.}, \tag{18}$$

where $\Omega_w = eB_w/mc$, and the $\mp$ sign denotes left-hand (right-hand) polarization of the wiggler. Comparing the static wiggler magnetic field Eq. (18) to the dynamic magnetic field of the pump,

$$\mathbf{B}_{\text{pump}} = \frac{mc^2k_0}{2e}(-ia_0e^{ik_0z - i\omega_0t}\mathbf{e}_+ + \text{c.c.}), \tag{19}$$

we see that we can replace a_0, k_0, and ω_0 in Eqs. (10) and (12) by $i\Omega_w/ck_w$, k_w, and zero, respectively, so as to calculate the steady-state solutions for the wiggler system in a straightforward manner. The amplitude of electron longitudinal motion for resonance ($\omega_1 = \Omega_0$) becomes

$$\widetilde{\zeta} = \frac{2ca_1}{\Omega_w}. \tag{20}$$

The steady-state transverse motion for detuned probe ($\omega_1 \neq \Omega_0$ and $\omega_p = \Omega_0$) is

$$\beta_+ = -\frac{i\omega_1a_1(\omega_1\Omega_w^2 - 2(\Omega_0 + \omega_1)^2\delta\Omega)}{2\omega_1^2\Omega_w^2 - 2(\Omega_0 + \omega_1)^2\delta\Omega^2}e^{i\theta_1}$$
$$+ \frac{i\omega_1^2a_1^*\Omega_w^2}{2\omega_1^2\Omega_w^2 - 2(\omega_1 + \Omega_0)^2\delta\Omega^2}e^{-i\theta_1 \mp 2ik_wz}. \tag{21}$$

The dispersion relation is derived using $(c^2\partial_z^2 - \partial_t^2)\mathbf{E}_1 = 4\pi\partial_t\mathbf{J}$ and the $e^{i\theta_1}$ component of $\mathbf{J}$ calculated from Eq. (21):

$$\omega_1^2 = c^2k_1^2 - \omega_p^2\omega_1\frac{\delta\Omega - \Omega_w^2/8\Omega_0}{\Omega_w^2/4 - \delta\Omega^2}. \tag{22}$$

Here, only weak detuning ($\delta\Omega/\omega_1 \ll 1$) is considered and $\Omega_w^2\delta\Omega$ was ignored.

Perfect transparency ($\omega_1 = ck_1$) is achieved for a finite detuning $\delta\Omega = \Omega_w^2/8\Omega_0$. This is a consequence of our choice of $\Omega_0 = \omega_p$. In reality, the effective plasma frequency $\bar{\omega}_p \approx \omega_p + \Omega_w^2/8\omega_p$ in the presence of the wiggler is slightly higher. Therefore, exact resonance requires that both the cyclotron frequency Ω_0 and the probe frequency $\omega_1 = \bar{\omega}_p$ be slightly higher, in agreement with Eq. (22).

B. Temporal evolution of the longitudinal motion

In Sec. II A, we derived the steady-state motion of a single electron interacting with electromagnetic waves and a longitudinal harmonic field. The existence of the steady-state solutions is ensured by Eqs. (10) and (20). In this section, we investigate the temporal trajectory from the initial state ($\widetilde{\zeta} = 0$) to the steady state.

Replacing ζ by Eq. (8), we arrange the driving terms of Eq. (6) as pump, lower sideband, probe, and upper sideband:

$$\dot{\beta}_+ + i\Omega_0\beta_+ = -\omega_0a_0e^{i\theta_0} + \frac{i}{2}k_0(\omega_1 - 2\omega_0)a_0\widetilde{\zeta}{}^*e^{i(2\theta_0 - \theta_1)}$$
$$- \omega_1a_1e^{i\theta_1} - \frac{i}{2}k_0\omega_1a_0\widetilde{\zeta}e^{i\theta_1}, \tag{23}$$

where $\widetilde{\zeta}$ and a_1 are slowly varying amplitudes. We assume that the electron is already in steady state with the pump. Another assumption is that the electron responds to the lower sideband in quasi-steady manner, i.e., the electron motion driven by the lower sideband is always in steady state, with its amplitude changing slowly in accordance with $\widetilde{\zeta}{}^*(t)$ given by the third term on the RHS of Eq. (9). The solutions of β_+ driven by the pump and the lower sideband are the same as in the previous section. No steady state can be assumed, however, for the resonant driving terms (the probe and the upper sideband). Instead, the transverse motion is decomposed into the product of a slowly varying amplitude $\widetilde{\beta}_+(t)$ and a fast oscillation $e^{i\theta_1}$. The equation for $\widetilde{\beta}_+(t)$ becomes $d\widetilde{\beta}_+/dt = -\omega_1a_1 - ik_0\omega_1a_0\widetilde{\zeta}/2$, which yields

$$\widetilde{\beta}_+(t) = -\omega_1\int_0^t(a_1(t') + ik_0a_0\widetilde{\zeta}(t')/2)dt'. \tag{24}$$

Equation (24) is approximate because it neglects the dependence of θ_1 on the longitudinal displacement ζ. The transverse motion is a superposition of electron responses to each driving term:

$$\beta_+ = \frac{i\omega_0a_0}{\Omega_0 - \omega_0}e^{i\theta_0} + \frac{k_0(\omega_1 - 2\Omega_0)a_0\widetilde{\zeta}{}^*}{2(\Omega_0 - 2\omega_0 + \omega_1)}e^{i(2\theta_0 - \theta_1)} - \omega_1e^{i\theta_1}$$
$$\times \int_0^t\left(a(t') + \frac{ik_0a_0}{2}\zeta(t')\right)dt'. \tag{25}$$

The difference between Eq. (25) and the steady state Eq. (9) is the treatment of the adiabatic turn-on of the probe field in Eq. (25).

Substituting Eqs. (8) and (25) into Eq. (7) yields an equation for the envelope $\widetilde{\zeta}(t)$:

$$\ddot{\widetilde{\zeta}} - 2i\Delta\omega\dot{\widetilde{\zeta}} = c^2k_0\omega_1a_0^*\int_0^t\left(a_1(t') + \frac{ik_0a_0}{2}\widetilde{\zeta}(t')\right)dt'$$
$$+ ic^2k_1a_1a_0^*\frac{\omega_0}{\Delta\omega} - \frac{c^2k_0^2|a_0|^2}{4}\left(\frac{\omega_1 + 2\omega_0}{\Delta\omega}\right)\widetilde{\zeta}, \tag{26}$$

where $\Delta\omega = \omega_1 - \omega_0$ and Ω_0 was replaced by ω_1 since resonance is considered. For a given pulse form of the probe
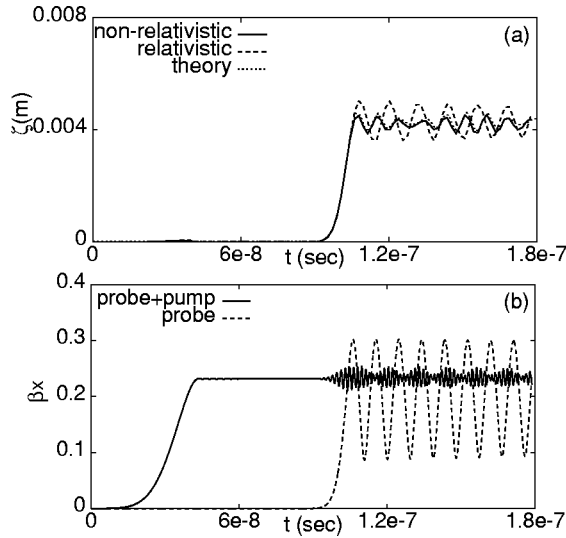
FIG. 1. (a) Temporal evolution of $|\widetilde{\zeta}(t)|$ from theory (dotted line) given by Eq. (27), non-relativistic single particle simulation (solid line), and relativistic simulation (dashed line). (b) Time trace of $|\beta_\perp|$ from a single particle simulation with the same parameters when the electron is driven by the pump and probe (solid line) and only by the probe (dashed line). The parameters are $a_0 = 0.05$, $\omega_1 = \Omega_0$, $\omega_0 = 0.8\Omega_0$, and $B_0 = 0.1$ T. The probe envelope is $0.005 \exp(-(t-300\lambda_1/c)^2/(20\lambda_1/c)^2)$.

$a_1(t)$, the time evolution of $\widetilde{\zeta}(t)$ can be obtained from Eq. (26). Differentiating both sides of Eq. (26) converts the integral equation into a third-order ordinary differential equation:

$$\widetilde{\zeta}''' + A\widetilde{\zeta}'' + B\widetilde{\zeta}' + C\widetilde{\zeta} = F(t), \tag{27}$$

where $A = -2i\Delta\omega$, $B = (c^2 k_0^2 |a_0|^2/4)(\omega_1 + 2\omega_0)/\Delta\omega$, $C = -ic^2 k_0^2 \omega_1 |a_0|^2/2$, and

$$F(t) = c^2 k_0 \omega_1 a_0^* a_1(t) + ic^2 k_1 (\omega_0/\Delta\omega) a_0^* \frac{da_1(t)}{dt}. \tag{28}$$

Note that Eq. (28) is a driving term determined by the envelope of the probe.

A numerical solution to the adiabatic Eq. (27) is compared in Fig. 1 to a single particle simulation. In the simulation, we solved Eqs. (2) and (3) using a modified version of the one-dimensional OOPIC,[13] for which a harmonic longitudinal electric field ($E_z = -\omega_p^2 \zeta$) was implemented and a single particle was loaded. The parameters used in Fig. 1 are $a_0 = 0.05$, $a_1 = 0.005$, $\omega_0 = 0.8\Omega_0$, $\omega_1 = 1.0\Omega_0$, and $B_0 = 0.1$ T. The front of the probe has an envelope given by $a_1 \exp(-(t-300\lambda_1/c)^2/(20\lambda_1/c)^2)$, where $\lambda_1 = 2\pi c/\omega_1$. The probe amplitude at the entrance to the plasma is taken to be constant for $t > 300\lambda_1/c$. The front of the pump has an envelope $a_0 \exp(-(t-120\lambda_1/c)^2/(40\lambda_1/c)^2)$. The delay of the probe is such that plasma electrons reach steady-state motion in the pump before the probe enters the plasma. Figure 1(a) shows the behavior of $|\widetilde{\zeta}(t)|$ predicted by theory and by a non-relativistic simulation. Initially $|\widetilde{\zeta}(t)| = 0$; in the presence of the pump and probe it grows until it has small fluctuations about a steady-state value $|\widetilde{\zeta}| = 2a_1/k_0 a_0 = 0.0043$. Higher fluctuation is observed in a relativistic

simulation. The perpendicular speed of the electron is about $|\beta_\perp| \sim 0.2$, as in Fig. 1(b), from which the relativistic factor is $\gamma = 1.02$. The change in the relativistic cyclotron frequency, Ω_0/γ, is about 2%, which yields a comparable change in $|\widetilde{\zeta}|$ in the relativistic case. Figure 1(b) shows that $|\beta_\perp|$ remains at the saturation level driven by the pump, which implies that the resonant motion driven by the probe is well suppressed. As expected, $|\beta_\perp|$ reaches a much higher value in the absence of the pump, although the relativistic effects naturally prohibits it from increasing indefinitely. The fluctuation level in ζ can be lowered by making the probe envelope more adiabatic.

III. SIMULATION RESULTS

In this section, we present some major results of EIT simulations which include the numerical observation of EIT, and a comparison of theory and simulations.

The code used in our simulations is a one-dimensional version of the OOPIC.[13] This is a fully relativistic electromagnetic PIC code. The code is spatially one-dimensional and follows three velocity components, making it a useful tool to simulate transversely homogeneous electromagnetic problems. Diagnostics which separate the right- and left-moving waves are implemented in this code: the amplitude of the right-going wave is calculated as $E_{\text{right-going}} = E_x + cB_y$, where E and B represent the electric field and the magnetic induction and c is the speed of light. This procedure separates the fields exactly in the vacuum. The technique of splitting the electromagnetic waves into left- and right-propagating components has been used extensively for studying the interaction between counter-propagating lasers in plasmas.[14–16]

A. Plasma EIT

Transparency of the resonant probe is demonstrated in Fig. 2. Simulation parameters are as follows: probe amplitude $a_1 = 0.005$, pump amplitude $a_0 = 0.05$, $\omega_1 = \Omega_0$, $\omega_0 = 0.8\Omega_0$, and $\omega_p = 0.2\Omega_0$. The cyclotron frequency is $\Omega_0/2\pi = 3.0 \times 10^{10}$ Hz. We measured the propagation of the right-going wave envelope and the longitudinal wave inside the plasma slab. The oscillation pattern of the envelope originates from the beat between the pump and probe. At earlier times, in Fig. 2(a), there is no beat on the right side of the plasma. This implies that the probe has not been transmitted. As the longitudinal wave is excited in the whole region of the plasma [Fig. 2(d)], transparency of the probe is observed [Fig. 2(c)].

To verify that the transparency of the probe wave is induced by the interaction of the two waves inside the plasma, we tried probe-only and pump-only cases. The fast Fourier transform (FFT) of the electric field of the electromagnetic wave at the far end of plasma is shown for these cases in Fig. 2(e). The signal is very noisy and there is no clear peak at any frequency when the probe is launched without the pump. For the pump-only case, there is a single peak at the pump frequency. When the probe is launched along with the pump, there are two additional peaks other than the pump: one is at
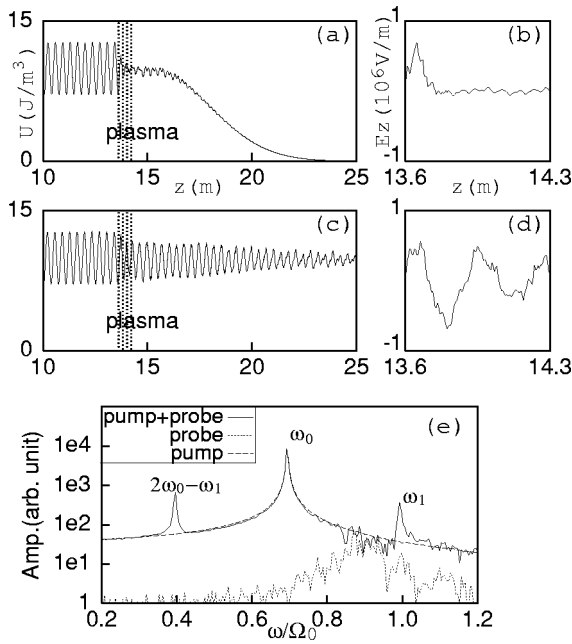
FIG. 2. Simulation results showing transparency at cyclotron resonance. The total wave energy density is shown at (a) $t = 1.06 \times 10^{-7}$ s, (b) $t = 1.40 \times 10^{-7}$ s. In (b) and (d) the corresponding longitudinal wave inside the plasma slab is plotted. This shows the excitation of the plasma wave is required for the transmission of the probe (see the text). (e) Fast Fourier transform (FFT) of $E(t)$ measured at the right-hand side of the plasma slab for *pump+probe* (solid line), *probe* (dotted line), and *pump* (dashed line).
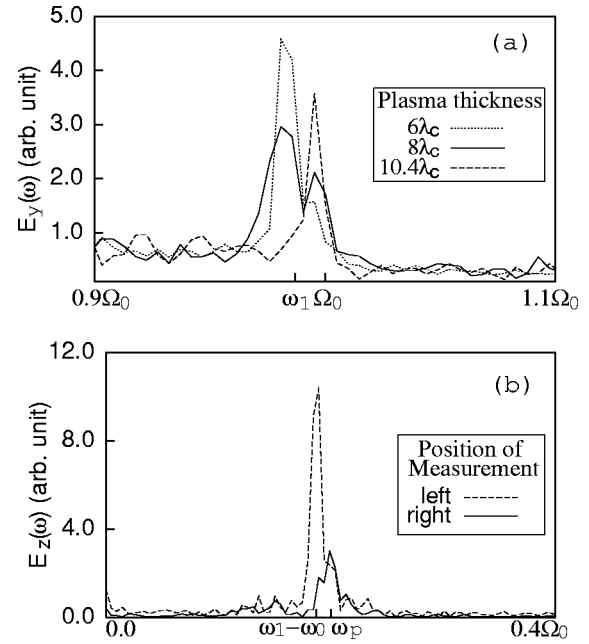

FIG. 3. The transparency of a probe detuned from the resonance is degraded as the plasma is made thicker. (a) FFT of the perpendicular electric field for a plasma thickness $6\lambda_c$ (dotted line), $8\lambda_c$ (solid line), and $10.4\lambda_c$ (dashed line) as measured beyond the right boundary of the plasma. λ_c is defined as $2\pi c/\Omega_0$. (b) FFT of the longitudinal electric field measured inside the plasma slab near the left plasma–vacuum boundary (dashed line) and the right boundary (solid line). The wave is incident on the left boundary and escapes through the right boundary.

the probe frequency, indicating transparency, and the second peak is at the lower sideband of the pump.

Another possible explanation of Fig. 2, other than EIT, is that the signal measured on the right side of the plasma slab originates from stimulated Raman scattering (SRS) of the pump. To distinguish the EIT from SRS, we simulated a probe slightly detuned from the cyclotron frequency. Figure 3(a) represents the FFT of transmitted signals which were measured with changing plasma thicknesses. The position of the measurement is separated by $8\lambda_1 = 8 \times 2\pi c/\omega_1$ from the plasma–vacuum boundary where the waves escape. The dominant peak appears at the probe frequency for a thin plasma. As the plasma becomes thicker, another peak grows at the cyclotron frequency, while the peak at the probe frequency is reduced. The frequency spectrum of the longitudinal wave measured at two different points inside the plasma is in Fig. 3(b). The dominant peak appears at $\omega_1 - \omega_0$ when it is measured near the plasma–vacuum boundary of wave incidence, while the main peak appears at the plasma frequency (ω_p) when measured far from that boundary. It is thought that, as the plasma becomes thicker, a wave at the cyclotron frequency is amplified via the SRS process and a resonant longitudinal wave with $\omega_p = \Omega_0 - \omega_0$ starts to dominate the plasma response to the pump+probe, at $\omega_1 - \omega_0$. Accordingly, the transparency channel of the probe, which is induced by the beat of the probe and pump, would be narrowed down resulting in the blocking of the probe transmission. The thickness at which EIT is not observable in simulations depends on the detuning and the plasma density. High density and larger detuning require narrower plasmas. The

typical maximum thickness for detuning $\omega_1 \sim 0.99\Omega_0$ and $\omega_p \sim 0.2\Omega_0$ was approximately $20\pi c/\Omega_0$.

The application to accelerators relies on the generation of a longitudinal electric field. An analytical expression can be obtained from Eq. (10) and $4\pi J = -\partial E/\partial t$:

$$\widetilde{E}_z \simeq \frac{2m\omega_p^2 a_1}{ek_0 a_0}. \tag{29}$$

Simulation results for $\widetilde{E}_z$ are summarized in Fig. 4, where $\widetilde{E}_z$ is plotted as a function of a_1/a_0. The field average from the simulation is calculated as a temporal mean value averaged over more than 50 oscillation periods of $\widetilde{E}_z(t)$ at the center of plasma. The error bars in Fig. 4 are the maximum and minimum peaks during the averaging interval. A linear fit to
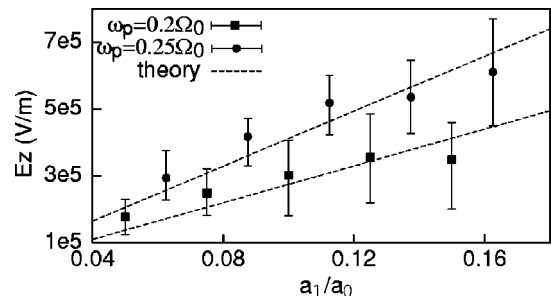

FIG. 4. Measurement of the average peak longitudinal field for $\omega_p = 0.2\Omega_0$ (squares) and $\omega_p = 0.25\Omega_0$ (circles). The error bars measure the variation of the peak field over the averaging time. The lines are from Eq. (29).
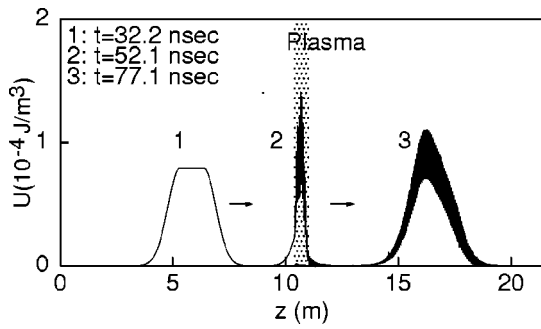
FIG. 5. Simulation of transparency in a system where the pump electromagnetic wave is replaced by a wiggler field. The probe energy density is shown at successive times, labeled 1, 2, and 3. Note the pulse compression in the plasma and the oscillation pattern on the envelope of the transmission (labeled 3). The pattern is from slight change in the probe from the circular to the elliptical polarization.

the data in Fig. 4 for $\omega_p = 0.25\Omega_0$ is 4.1×10^6, while the theoretical slope based on Eq. (10) is 4.3×10^6. For $\omega_p = 0.2\Omega_0$, the fitting and the theory slopes are 2.8 and 2.7 $\times10^6$, respectively. There is thus fine agreement between theory and simulations. Though not plotted in Fig. 4, we also examined the case of $\omega_p = 0.3\Omega_0$ and found that the simulation longitudinal field was about 30% less than theoretical value. This was not pursued in detail, but we speculate that undesired SRS from the pump reduced performance of the EIT at this higher plasma density.

B. Wiggler system

We now present simulation and theory of induced transparency with the pump replaced by a magnetic wiggler. A typical simulation in shown in Fig. 5, where EIT is evident. The parameters are $a_1 = 0.0001$, $k_w = 2\pi/0.1$ m^{-1}, $B_0 = 0.1$ T, and $B_w/B_0 = 0.8$. The three snapshots were taken at $t = 3.2\times10^{-8}$ s, $t = 5.2\times10^{-8}$ s, and $t = 7.7\times10^{-8}$ s.

Notable in Fig. 5 is the compression of the probe in the plasma, which occurs because its group velocity is much lower than the speed of light in vacuum. Discussion of the pulse compression in terms of photon number can be found elsewhere.[6,7] The probe stretches as it exits the plasma, but the envelope suffers some distortion in the process.

A dispersion relation was obtained from the simulations by measuring the wavenumber as a function of frequency. We used a FFT to determine the probe wavenumber inside the plasma. A plasma slab size large enough to contain more than 30 wavelengths was used in the simulations, and a FFT was then used to produce a well-defined wavenumber. The result of such a FFT is seen in Fig. 6(a) for a right-hand polarized wiggler and Fig. 6(b) for a left-hand polarized wiggler. Note that, other than the major peak at the probe wavenumber, k_1, there exist clear sub-peaks at $k_1 + 2k_w$. These sub-peaks are driven by the $e^{-i\theta_1 \mp 2ik_w z}$ component of the transverse electron current in Eq. (21).

Comparison of the dispersion relation inferred from the simulations to the theoretical dispersion, given by Eq. (22), is presented in Fig. 7. The theoretical group velocity at $\omega_1 = \Omega_0$ is, from Eq. (22), $0.17c$ for $B_w/B_0 = 0.8$ and $0.11c$ for $B_w/B_0 = 0.6$. The corresponding values defined by fitting the
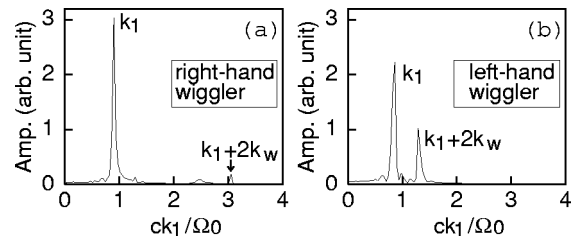

FIG. 6. Spatial FFT of the x-polarized electric field inside the plasma for (a) a right-hand wiggler and (b) a left-hand wiggler. The FFT was used to find the numerical dispersion relation in Fig. (7).

simulation data are quite close. Overall, the theory and simulation are in good agreement except for the case of a left-hand polarized wiggler which has $\lambda_w = 0.3$ m. A possible explanation for the difference in dispersion characteristics between the left- and right-hand polarization of the wiggler originates from the second term on the RHS of Eq. (21). This term was ignored in the derivation of the dispersion relation, since it is generally not resonant with the $e^{i\theta_1}$ component of the probe. However, at some specific values of λ_w, it may come close to resonance with the probe or with a higher harmonic. In such case the theory should be modified to include the new term (this is currently under study).

IV. THE WIGGLER EIT ACCELERATOR CONCEPT

The EIT interaction can be regarded as a method for inducing a longitudinal electric field in the plasma. The phase velocity of the longitudinal field is obtained by replacing θ_0 in Eq. (8) with $k_w z$, giving $v_\phi = \omega_1/(k_w \pm k_1)$. Using
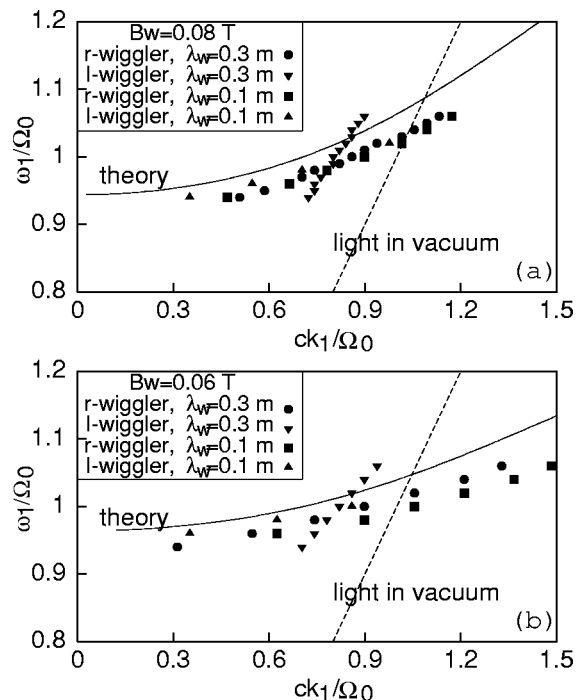

FIG. 7. Dispersion relation of probe in wiggler system for (a) $B_w/B_0 = 0.8$ and (b) $B_w/B_0 = 0.6$. Wiggler parameters are a right-hand polarized wiggler with $\lambda_w = 0.3$ m (circles), left-hand with $\lambda_w = 0.3$ m (inverted triangles), right-hand with $\lambda_w = 0.1$ m (squares), and left-hand with $\lambda_w = 0.1$ m (triangles).
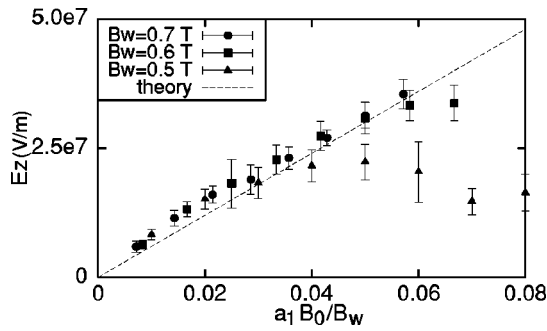
FIG. 8. $\tilde{E}_z$ vs $a_1 B_0 / B_w$ for $\lambda_w = 0.01$ m and $B_w = 0.7$ T (circles), 0.6 T (boxes), and 0.5 T (triangles). B_0 is fixed as 1 T. The solid line is from Eq. (31).

a wiggler with $\lambda_w = 0.5$ cm, one finds $\beta_\phi = 0.35c$, which is very slow compared to the phase velocity of the longitudinal field in other plasma-based advanced accelerators. For example, in the laser-wakefield accelerator the phase velocity of the longitudinal field equals the group velocity of the driving short laser pulse (or, roughly, $v_\phi / c = 1 - \omega_p^2 / 2\omega^2$). Thus, laser-wakefields are suitable for electron acceleration, but a poor choice, given present technology, for ion acceleration. In contrast, the slow phase velocity of the EIT accelerator makes them an interesting choice for ions or other heavy particles.

A remarkable characteristic of the wiggler-plasma system is that the phase velocity of the longitudinal wave is readily controllable. The amplitude of the longitudinal wave does not depend on k_w. Therefore, it is possible to control v_ϕ, keeping the wave level fixed, by simply adjusting the wiggler wavelength. The wavenumber of the probe inside the plasma at resonance ($\omega_1 = \omega_p = \Omega_0$) is, from Eq. (22), $k_1 = \omega_1 / \sqrt{2}c$. Then,

$$\beta_\phi = \frac{v_\phi}{c} = \frac{1}{1/\sqrt{2} + \lambda_v / \lambda_w}, \qquad (30)$$

where λ_v is the wavelength of the probe in vacuum. An axial magnetic field of 1 T corresponds to a probe frequency $\omega_1 = \Omega_0 = 1.76 \times 10^{11}$ or wavelength $\lambda_v = 1.07$ cm. As ions accelerate it may be useful to change the phase velocity. Simulations (not shown) confirm the result that the phase velocity given by Eq. (30) is readily controlled by tapering the wiggler wavelength.

An important figure of merit for any accelerator is the accelerating gradient. For the EIT accelerator, the gradient is readily calculated using $4\pi J_z = -\partial E_z / \partial t$ and Eq. (20):

$$\tilde{E}_z = a_1 \frac{2mc\omega_p^2}{e\Omega_w}. \qquad (31)$$

Recall that, in the case of the wiggler EIT, $\omega_p = \Omega_0$. Hence, Eq. (31) shows that $\tilde{E}_z$ is proportional to the product of a_1 and the ratio of B_0 to B_w for a given value of B_0. It is natural to plot, as seen in Fig. 8, the measured $\tilde{E}_z$ (from simulations) as a function of $a_1 B_0 / B_w$. Simulation results are shown for

$B_0 = 1$ T, $B_w = 0.5$, 0.6, 0.7 T, and $\lambda_w = 0.01$ m. The axial magnetic field used in Fig. 8 is higher than the $B_0 = 0.1$ T used is earlier simulations. This change is motivated by the scaling of $\tilde{E}_z$ with B_0 seen in Eq. (31). A stronger axial field and corresponding higher plasma frequency result in increased accelerating gradients. The typical value we obtain for the longitudinal field is of order 10^7 V/m, which is of interest for an ion accelerator. For values of $a_1 B_0 / B_w < 0.04$, simulation results agree very well with Eq. (31). The linear theory fails as $a_1 B_0 / B_w$ increases because of the large amplitude of the plasma wave, which is of order $\delta n / n \sim 0.3$ for $a_1 B_0 / B_w \sim 0.05$.

V. SUMMARY

We presented the theory and simulation of EIT in a magnetized plasma. The transparency of the resonant wave was clearly seen in the one-dimensional PIC simulations of EIT using an electromagnetic and wiggler pump. A dispersion relation was derived including the influence of the upper and lower sidebands of the pump. Analytic expressions for the longitudinal plasma field and the transverse electron motion were obtained. The analytic results for the dispersion relation and the longitudinal field were shown to be in agreement with PIC simulations. The wiggler-based system can be used to excite accelerating fields with controllable phase velocity and a gradient ≥ 20 MeV/m. Further detailed studies are under way to determine the performance limits of an ion accelerator based on this concept.

ACKNOWLEDGMENTS

[1] K. J. Boller, A. Imamoglu, and S. E. Harris, Phys. Rev. Lett. **66**, 2593 (1991).
[2] S. E. Harris, Phys. Rev. Lett. **70**, 552 (1993); Phys. Today **50** (7), 36 (1997).
[3] L. V. Hau, S. E. Harris, Z. Dutton, and C. H. Behroozi, Nature (London) **397**, 594 (1999).
[4] M. D. Lukin, S. F. Yelin, and M. Fleischhauer, Phys. Rev. Lett. **84**, 4232 (2000).
[5] A. G. Litvak and M. D. Tokman, Phys. Rev. Lett. **88**, 095003 (2002).
[6] G. Shvets and J. S. Wurtele, Phys. Rev. Lett. **89**, 115003 (2002).
[7] G. Shvets and J. S. Wurtele, *Proceedings of Advanced Accelerator Concepts, 10th Workshop, Mandalay Beach, California, 2002*, edited by C. E. Clayton and P. Muggli (American Institute of Physics, Melville, 2002), p. 681.
[8] M. S. Hur, J. S. Wurtele, and G. Shvets, in Ref. 7, p. 802.
[9] S. E. Harris, Phys. Rev. Lett. **77**, 5357 (1996).
[10] D. F. Gordon, W. B. Mori, and C. Joshi, Phys. Plasmas **7**, 3145 (2000).
[11] D. F. Gordon, W. B. Mori, and C. Joshi, Phys. Plasmas **7**, 3156 (2000).
[12] E. Esarey, P. Sprangle, J. Krall, and A. Ting, IEEE Trans. Plasma Sci. **24**, 252 (1996).
[13] H. Usui, J. P. Verboncoeur, and C. K. Birdsall, IEICE Trans. Electron. **E83C**, 989 (2000).
[14] G. Shvets, N. J. Fisch, A. Pukhov, and J. Meyer-ter-Vehn, Phys. Rev. Lett. **81**, 4879 (1998).
[15] G. Shvets and A. Pukhov, Phys. Rev. E **59**, 1033 (1999).
[16] P. J. Mardahl, H. J. Lee, G. Penn, J. S. Wurtele, and N. J. Fisch, Phys. Lett. A **296**, 109 (2002).